Blistering and hydrogen retention in poly- and single-crystals of aluminum by a joint experimental-modeling approach

C. Quiros, J. Mougenot, R. Bisson, M. Redolfi, A. Michau, K. Hassouni, G. Lombardi

Blistering and hydrogen retention in poly- and single-crystals of aluminum by a joint experimental-modeling approach

C. Quiros, J. Mougenot, R. Bisson, M. Redolfi, A. Michau, K. Hassouni, G. Lombardi

Blistering and hydrogen retention in poly- and single- crystals of aluminum by a joint experimental-modeling approach

C. Quiros[a], J. Mougenot[a], R. Bisson[b], M. Redolfi[a], A. Michau[a], K. Hassouni[a], G. Lombardi[a,*]

[a] LSPM-CNRS, Université Paris 13, Sorbonne Paris Cité, 93490 Villetaneuse, France
[b] Aix-Marseille Univ, CNRS, PIIM, Marseille, France

ARTICLE INFO

Keywords:
Blistering
Aluminum
Hydrogen inventory

ABSTRACT

Aluminum samples have been exposed to a hydrogen plasma generated by a low-pressure – high-density microwave reactor. Aluminum has been chosen as a surrogate for Beryllium. The fluence was kept below 4×10^{24} ions/m^2, in order to study the first steps of nucleation and growth of surface and bulk defects, *i.e.* blisters and bubbles. Experimental analyzes and macroscopic rate equation (MRE) modeling on poly- and single-crystals were made to investigate the role played by grains boundaries in the hydrogen retention. Temperature programmed desorption (TPD) on Al poly-crystals revealed the production of aluminum hydrides (alanes) as majority species in the desorption flux. Comparison of microscopy observations for three different single-crystal orientations (⟨100⟩, ⟨110⟩ and ⟨111⟩) allowed to determine preferential orientations able to attenuate the formation of blisters.

1. Introduction

Plasma-wall interactions present a serious concern in existing and future fusion reactors. Surface modification of plasma facing components (PFCs), and hydrogen retention are some of the problems that must be resolved before achieving economically and regulatory sustainable nuclear fusion. Beryllium (Be) has been chosen as a first wall material for ITER due to its high thermal conductivity, low neutron activation, low Z and its affinity with oxygen [1,2]. However the dusts and powders made of Be are highly toxic, and must be avoid during Tokamak operation. Among other materials like chromium and copper [3,4], aluminum (Al) is a possible less toxic proxy material to Be, which presents some similar behavior after plasma exposure [4–8]. Its studies can therefore provide useful information that can be later adapted to Be. In this paper, experimental and modeling results are shown for hydrogen retention and blister formation in crystals of Al.

Hydrogen exposure of aluminum samples leads to different modifications on its surface and in its bulk. To study these effects, the samples have been placed in a dedicated low-pressure – high-density electron cyclotron resonance microwave plasma reactor described elsewhere [8,9], able to generate a hydrogen ion flux of $\sim 1.6 \times 10^{20}$ ions/m^{2}s, thanks to a ionization efficiency ranging from 10^{-4} to 10^{-3}. As an illustration, scanning electron microscope (SEM) pictures are given Fig. 1a and b that show, respectively, the surface, and the cross-section of an Al poly-crystal sample after being exposed to low pressure (0.1 Pa) hydrogen plasma at a fluence of 1.3×10^{24} ions/m^2 with 320 eV incident ion energy (to induce trap creation), and a surface temperature of 618 K (induced by the plasma, measured by a pyrometer). It can be observed in Fig. 1a a high density of blisters on the Al surface, with sizes in the range 2–30 μm. The grain boundaries structure was determined through electron backscattering diffraction (EBSD) measurements (not shown here). These blisters are located either at the grain boundaries, *i.e.* intergrain blisters or within the grains, *i.e.* intragrain blisters. The surface exhibits a slight swelling in many regions of the sample. The cross-section on Fig. 1b shows large irregular cavities and circular bubbles in the bulk of the sample. For the analyzed conditions, bubbles are formed at a maximum depth of 80 μm whereas irregular cavities were mostly located at the grain boundaries and at depths of up to 90 μm.

There have been multiples studies explaining differences between bubbles, blisters, cracks, cavities and voids is literature [10]. The term bubbles refers to quasi-spherical shaped cavities in the bulk of the material whereas blisters consist of dome-shaped deformations of the material surface with mostly circular, but sometimes, irregular circumference (see Fig. 1a). Underneath blisters one may find a spherical shaped bubble (along the cutting direction), a lenticular cavity or a crack (see Fig. 1b).

In the following sections will be presented results obtained first on Al poly-crystals, then Al single-crystals. Both have been purchased at Goodfellow, with a purity of 99.99%. Their dimensions are 1 cm in

* Corresponding author.
E-mail address: lombardi@lspm.cnrs.fr (G. Lombardi).

https://doi.org/10.1016/j.nme.2019.100675

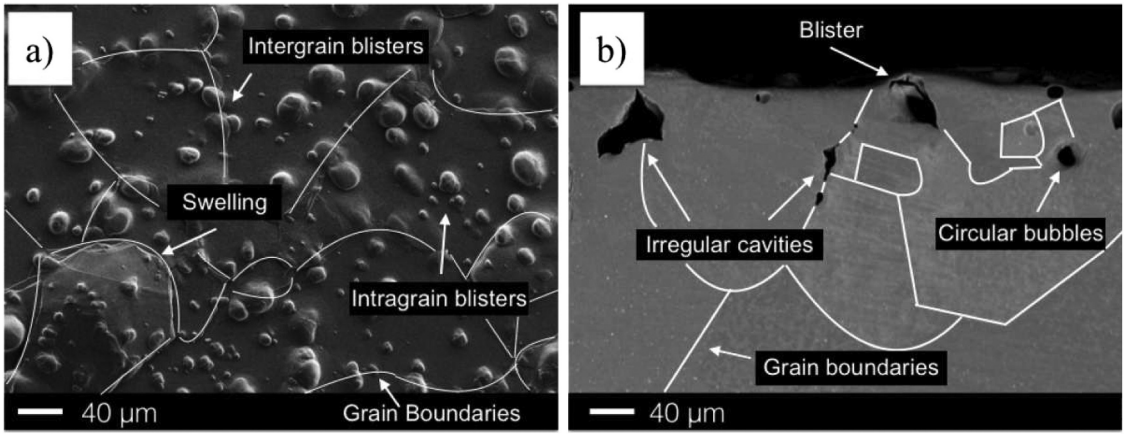

Fig. 1. (a) Blisters at the surface, (b) bubbles and cavities in the bulk (cross-section) of an aluminum sample after hydrogen plasma exposure with flux of 1.6×10^{20} ions/m^{2}s, fluence of 4.7×10^{24} ions/m^2 and incident ion energy of 320 eV.

diameter and a thickness of 2 mm. Poly-crystals and single crystals have been polished to a mirror-like finish (roughness $R_a \sim 20$ nm) first by a mechanical polishing with an abrasive fine-grained silicon carbide (SiC) grinding paper, then thanks to a chemo-mechanical process performed using an active oxide polishing suspension (OPS) which uses Coloidal Silicia (SiO_2) as an abrasive. Poly-crystals were annealed for 2 h at 673 K at a pressure of 10^{-4} Pa to obtain grains larger than 100 µm. Single-Crystals were also annealed to reduce the number of dislocations. To avoid the formation of a native oxide layer at the surface, when not exposed to the plasma, the samples were kept under vacuum conditions or in absolute ethanol. Nevertheless a thin ($\sim$ 10 nm), stable, passivating oxide layer even under vacuum conditions remain possible [2], although not investigated in this paper.

2. Studies on Al poly-crystals

In a previous combined experimental and modeling effort [8], we developed macroscopic rate equation (MRE) models for Al and Be that described hydrogen retention at dislocations and vacancies as well as bubble growth. We were able to reproduce the bubble growth kinetic in Al poly-crystals and the absolute hydrogen retention in Be poly-crystals. Our goal here was to model both deuterium (D) retention and bubble growth on Al poly-crystals, at least in an *ad hoc* manner. Indeed, only a few first principles study exist regarding hydrogen interaction with Al defects [11], thus the use of a global approach for Al, such as recently employed for tungsten [12], may be too premature. We attempted the development of an *ad hoc* model combining (i) experiments on D implanted Al poly-crystal with D retention quantification by means of a calibrated temperature programmed desorption (TPD) setup in a line-of-sight configuration [13], with (ii) the 1-D macroscopic rate equations (MRE) code HIIPC used to simulate hydrogen retention in materials and bubble formation [8,14,15]. The aim was to compare the TPD spectra with the MRE model known to describe correctly the bubble growth in Al [8], *i.e.* including vacancies and dislocations but not grain boundaries trapping.

An Al poly-crystal has been exposed to deuterium plasma with fluence of 3×10^{23} ions/m^2 (incoming flux of 1.7×10^{20} ions/m^{2}s), incident ion energy of 320 eV and surface temperature of 618 K. After the D implantation, the sample was shipped to the TPD setup, Al being in ambient atmosphere for 3 days, allowing a slow migration of D in and out of Al. Finally, the TPD spectra were recorded with a temperature ramp of 1 K/s. The comparison of the TPD experiment and the MRE model is presented in Fig. 2a). In experiments (black), deuterium desorption starts around 360 K and the maximum peak desorption is reached around 700 K. MRE modeling agrees with experiments regarding the desorption peak temperature. However, there is negligible desorption below 500 K in the simulation, in contrast to the experimental observation. This difference could indicate that grain boundary trapping plays a role in D retention. However, such conclusion cannot be reached because hydrogen release from Al appeared to be more complicated than anticipated. Winkler et al. showed that Al hydrides are minority products for hydrogen atom fluence of 10^{19} atoms/m^2 when the temperature ramp used in TPD remains below 3 K/s [16]. This is the reason we selected a 1 K/s ramp to perform TPD here but it appeared to be not sufficient to avoid important Al hydrides emission from the sample. Fig 2b) presents the calibrated TPD results for HD, D_2, D_2O and AlD species that amount for a deuterium retention of 1.1×10^{20} D/m^2. Note that to convert the raw signal of AlD in a quantified desorption flux only a theoretical total ionization cross section is available in the literature [17]. For Al poly-crystal exposed to about 10^{23} ions/m^2, it appears that at least 80% of the desorbed D is in the form of AlD. We stress that we can only give a lower limit since Al, AlD_2, AlD_3 and Al_2D_y alanes have been also detected. However, the absence of any partial ionization cross section in the literature prevent the quantification of these species and thus any accurate D retention, explaining the difference of retention by a factor of $\sim$10 between TPD experiments and MRE simulation (Fig 2a). Thus, future inclusion of TPD experiments in MRE modeling of hydrogen – aluminum interactions should first solve the problem of formation and/or quantification of aluminum hydrides at fusion relevant fluence.

Putting the issue of retention quantification aside, we continued to investigate the role of grain boundaries on retention and bubble formation by probing the effect of grain boundary misorientation. To perform this study two samples were analyzed: a non-textured sample and a ⟨100⟩ textured sample as determined by EBSD measurements. Both samples were exposed to a continuous plasma treatment with the same conditions than described above (H_2 plasma with an incident ion flux of 1.6×10^{20} ions/m^{2}s, sample temperature of 618 K, incident ion energy to the biased sample of 320 eV). The fluence was fixed at 2.8×10^{24} ions/m^2. Fig. 3a and b show respectively SEM micrographs of the non-textured and the textured Al sample. The non-textured sample shows a lower blister density than the textured sample, but with larger size: statistical measurements give a blister density of 160 blisters/mm^2, with an average radius of 8 µm for the non-textured sample whereas the textured sample has a blister density of 5000 blisters/mm^2 with an average radius of 2.5 µm.

For the analyzed fluence, blister growth in the textured samples occurs in the grains (*i.e.* intragrain blisters) whereas blister growth in the non-textured sample occurs mainly at the grain boundaries (*i.e.* intergrain blisters). Boundaries act as traps for hydrogen and since H-atoms are not bonded to the maximum number of aluminum atoms, it is easier for blisters to grow in this area through loop punching and plastic

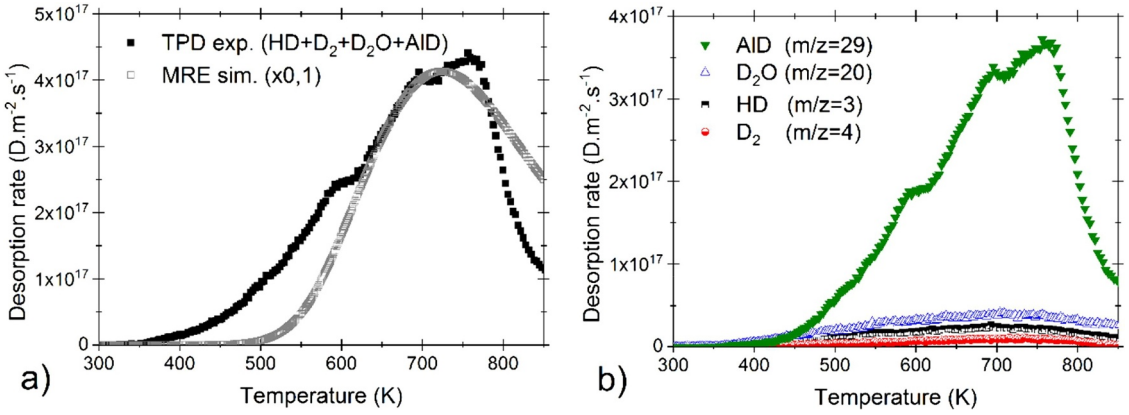

Fig. 2. (a) TDP measurements (HD, D_2 and D_2O products) and MRE simulation of a poly-crystalline Al sample after exposure to deuterium plasma with fluence of 3×10^{23} ions/m^2. (b) desorption rate measured for AlD, D_2O, HD and D_2 products.

deformation [18–20].

EBSD analysis showed that the misorientation angle between adjacent grain boundaries plays a key role in blister appearance [8]. Intergrain blisters were mainly located at the grain boundaries with a misorientation angle higher than 15° degrees. On the other hand, textured samples showed the opposite behavior.

Since the blistering kinetics is much faster at the grain boundaries of non-textured samples with respect to textured samples, it is relevant to analyze single crystal aluminum samples to have a better understanding of the intragrain blister growth, as it will be presented in the next section.

3. Studies on Al single-crystals

In order to analyze the effect crystallographic orientation has on blister nucleation, experiments were performed on three aluminum single crystal (ASC) samples respectively named ⟨100⟩, ⟨110⟩ and ⟨111⟩ ASC. These samples were purchased from Goodfellow and their dimensions are: 10 mm in diameter and a thickness of 2 mm

Prior to plasma exposure the samples were polished to a mirror-like finish. Afterwards they were exposed to H_2 plasma with an incident ion flux of 1.6×10^{20} ions/m^2s, sample temperature of 618 K, fluence of 2×10^{23} ions/m^2 and incident ion energy to the biased sample of 320 eV.

After plasma exposure the samples were analyzed with a confocal optical microscope given that it has a higher height resolution than the SEM. We made use of a Keyence VK-9700 Laser Scanning Confocal Microscope, whose height accuracy is as low as 10 nm. This allows analyzing blister morphology in greater detail.

After hydrogen plasma exposure, the sample surface shows the growth of blisters with a different morphology and size depending on the crystallographic direction of the sample, as shown in Fig. 4. The ⟨100⟩ ASC shows blisters with a square-like morphology, the ⟨110⟩ ASC shows ellipsoidal-shaped blisters and the ⟨111⟩ ASC shows mostly triangular blisters.

As for blister size, the ⟨111⟩ ASC sample shows the smallest blisters with an average radius of 3.0 μm and average height of 4.2 μm, the ⟨100⟩ ASC sample shows blisters with an average radius of 5.3 μm and average height of 8.4 μm, and the ⟨110⟩ ASC sample shows blisters with an average radius of 15.2 μm and an average height of 41.7 μm. We focused or study on the morphology of the blisters rather than their concentration, but we nevertheless observed a dependence of the concentration related to the blister volume (higher volume leads to lower surface concentration).

It is worthy to mention that in crystalline materials plastic deformation occurs by the motion of dislocations in a process called slip. Dislocations do not move freely in every crystallographic direction. They usually have a preferred plane, known as slip plane. In this slip plane there are specific directions, known as slip directions, along which dislocation motion is possible. The combined system consisting of the slip plane and the slip direction is referred to as slip system [21].

One can notice in Fig. 4 that blisters have terraces and steps. If the loop punching mechanism is valid, the plastic deformation experienced by blisters during growth should lead to the emergence of slip planes at the sample surface. As a result, blisters should have the terraced structure seen in Fig. 4. This terraced structure and hence the obtained

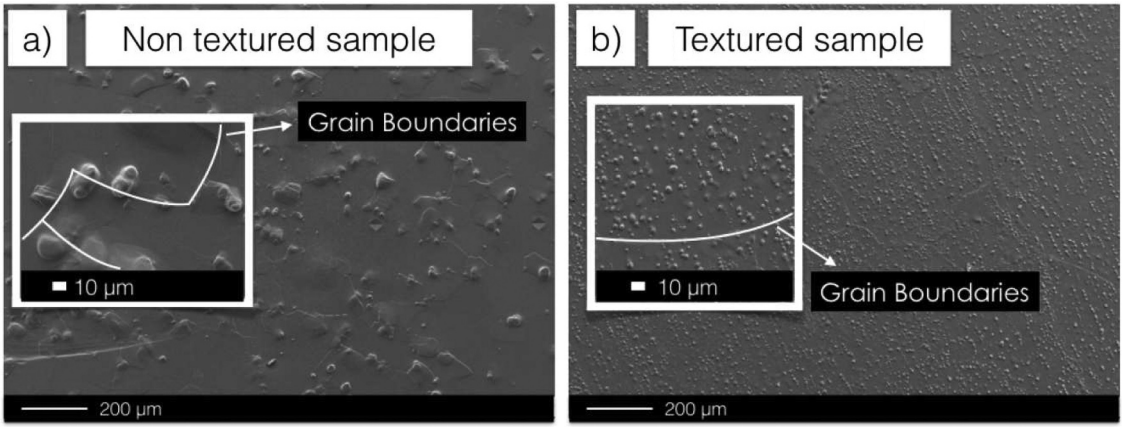

Fig. 3. SEM micrographs (a): non-textured and (b): textured Al (⟨100⟩) samples exposed to H_2 plasma with flux of 1.6×10^{20} ions/m^2s, fluence of 2.8×10^{24} ions/m^2 and incident ion energy of 320 eV.

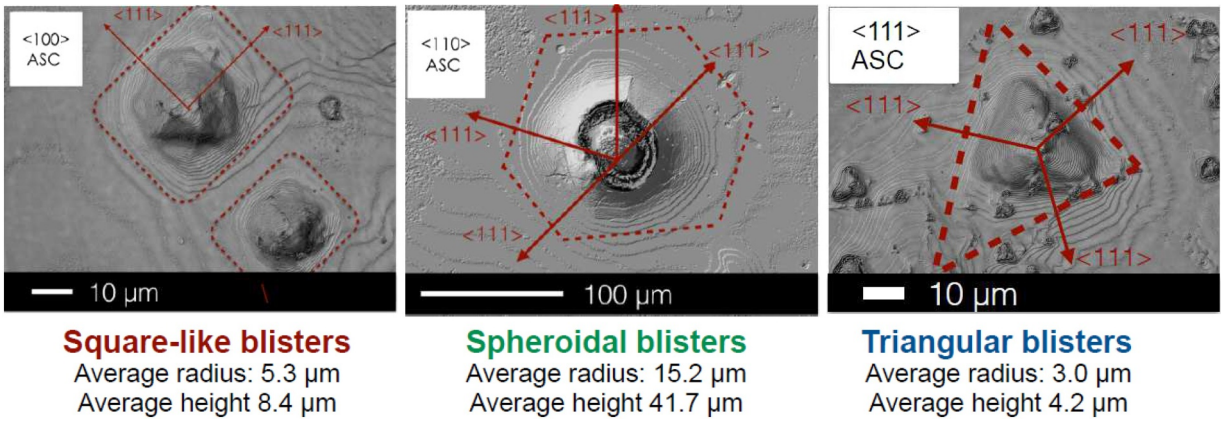

Fig. 4. Confocal images of the ⟨100⟩ (left), ⟨110⟩ (center) and ⟨111⟩ (right) ASC samples exposed to H_2 plasma with an incident ion flux of 1.6×10^{20} ions/m^{2}s, sample temperature of 618 K, incident ion energy of 320 eV and fluence of 2×10^{23} ions/m^2. The scale is not the same in every image.

blister morphology should be coherent with the slip system of the sample. Blister morphology should correspond to the macroscopic traces of the atomic scale crystallographic planes. The different shapes of the blisters and their discrimination are done using a comparison with stereographic projection for cubic crystals tilted to coincide with the analyzed direction of the Aluminum Single Crystal (ASC) [21]. In the case of a fcc material, such as aluminum, the slip systems correspond to the slip direction ⟨110⟩ and the slip plane {111}. This means that during plastic deformation of a fcc material the activated slip planes are the {111} planes. These planes are able to move in the ⟨110⟩ directions belonging to this plane. For each {111} slip plane, there are three ⟨110⟩ slip directions [21].

As mentioned, the exposure of ASC to hydrogen plasma showed that blister growth is affected by the crystallographic structure of the material: ⟨100⟩ ASC samples shows somewhat square-like shaped blisters, ⟨110⟩ ASC samples show mostly spheroidal blisters and finally ⟨111⟩ ASC samples show mainly triangular-shaped blisters. It was determined that spheroidal blisters in the ⟨110⟩ ASC should actually have an hexagonal shape, however there is a slip plane overlapping due to the plastic deformation experienced by the material.

The step or terraced structure observed in blisters is a consequence of the punching of dislocation loops during the growth process. These steps correspond to the slip plane of the material and their normal direction (ND) forms a well-defined angle with the surface ND. This angle may be estimated using the corresponding stereographic projection for each sample. The experiments performed with aluminum single crystals confirm that the angles are consistent with the values given by the stereographic projection. Thus confirming that blister growth is due to loop punching and that in fact, blister steps correspond to the macroscopic traces of the atomic scale crystallographic planes of the sample.

A sketch of the different blisters found in the ASC samples is shown in Fig. 5. This figure shows that under stress, plastic deformation occurs in the directions determined by the slip planes. As a result, in the case of a 90° degree angle between the slip direction and the sample surface, growth perpendicularly to the surface is enhanced. Therefore, blisters in the ⟨110⟩ sample (Fig. 4 center and Fig. 5c) are able to grow higher whereas blisters in the ⟨111⟩ sample reach the smallest heights.

4. Discussion and main conclusions

In this study, aluminum samples exposed to hydrogen plasma were subject to high energy ion implantation. Once implanted in the material the hydrogen diffuses and agglomerates in defects such as vacancies (v), cracks or grain boundaries. At relatively high fluences, as is the case in our experimental conditions, along with the low hydrogen solubility in aluminum [22], hydrogen concentration is generally able to reach high levels in the near surface regions. Hydrogen trapped in the material is able to agglomerate into hydrogen-vacancy (H_2-v) clusters, which marks the initial nucleation mechanism for bubbles [23,24].At high enough incident ion energies (more than 200 eV), implantation should create vacancies in the material [18,21]. Additionally, the presence of hydrogen in the material decreases the formation energy for vacancy creation, promoting the formation of H_2-v clusters. The combination of these two phenomena contributes to blister nucleation. This is the reason we performed the experiments at 320 eV of incident energy ions, to warranty blister nucleation.

Once a H_2-v cluster is formed, it has to increase in size to become a bubble. The critical pressure P under which bubbles can grow in the material is determined by the following equation [25], $P = E_t/\Delta V$, where E_t is that total energy of binding an existing cluster to a newly created vacancy (*i.e.* the formation energy of a vacancy plus the binding energy of a vacancy to a cluster) and ΔV is the change in volume which in this case corresponds to the volume of a vacancy. For hydrogen in aluminum, the formation energy of a vacancy is 0.67 eV [26], the binding energy of a single vacancy to a vacancy cluster is − 0.5 eV [27] and the volume of a vacancy is 6.89×10^{-30} m^3 [21]. The calculated critical pressure under which a bubble may form in aluminum is 3.95 GPa. However, this value was calculated under the condition that vacancies are at thermodynamic equilibrium at a certain temperature. If vacancies are superabundant because of a high hydrogen ion flux, the critical hydrogen pressure decreases drastically given that clusters may grow due to the binding energy. This can be observed by comparing the binding energy of a single vacancy to a vacancy cluster in aluminum (− 0.5 eV) with the binding energy of hydrogen atoms to a cluster in aluminum (− 5 eV) [28].

Thus, once an H_2-v cluster is formed and stabilized, it is able to increase in size due to the high internal pressures. The high pressure forces are able to punch interstitial loops out of one side of the bubble and plastically deform the material [18,21]. The present experiments performed on aluminum single crystals showed that blisters have a step or terraced structure. This terraced structure is a consequence of the punching of dislocation loops during the growth process. The blister steps correspond to the macroscopic traces of the atomic scale slip plane of the material and their ND forms a well-defined angle with the surface ND.

Additionally, we showed that blister growth in aluminum is influenced by the sample microstructure. In non-textured samples, intragrain blister nucleation kinetics occurred much slower than intergrain blister kinetics. As the misorientation angle between adjacent grain boundaries decreases, so does the dislocation centers at the grain boundaries. As a result, for smaller misorientation angles it is harder for blisters to grow in this area through loop punching and plastic deformation. For the analyzed conditions, blisters in textured samples appeared only within the grains.

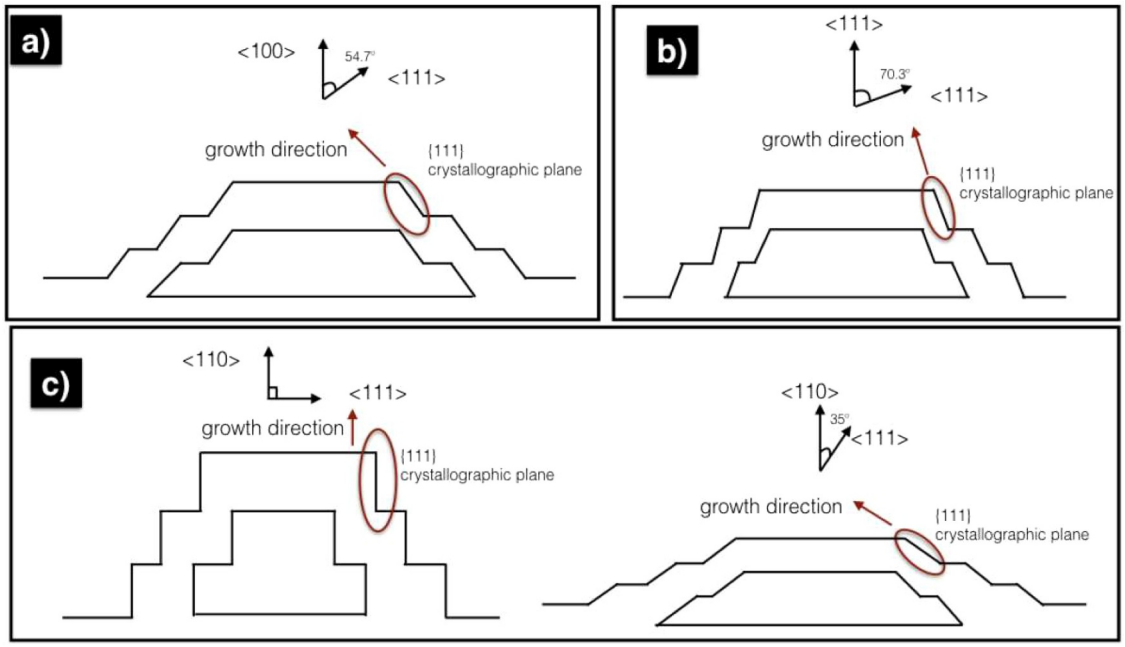

Fig. 5. Model of blister growth through plastic deformation for the (a) ⟨100⟩, (b) ⟨111⟩ and (c) ⟨110⟩ single crystals. Blister steps are directed with respect with the direction normal to the surface with an angle of (a) 54.7∘, (b) 74.3∘ and (c) 90∘ and 35∘, respectively. The higher the angle, the higher will be the blister height.

The present information obtained on the complex blister growth in aluminum could be included in future MRE models dedicated to forecast more accurately hydrogen retention in Be-like materials. To do so, a link between bubble nucleation and hydrogen retention is necessary. We attempted to create such a link using TPD quantification of hydrogen in Al at fluence where bubble nucleation starts. For a hydrogen fluence of $\sim 10^{23}$ ions/m^2, aluminum hydrides were found to be majority species in TPD, preventing an accurate determination of retention because only the AlH molecule can be quantified. It should be stressed that this dominant hydride emission was unexpected on aluminum because it is at variance with the literature performed at lower fluence, typically $\sim 10^{19}$ atoms/m^2 [29]. To our knowledge, the work of Lossev and Küppers discarded the emission of hydrides in the case of Be [30]. However, Lossev and Küppers' work was also realized in the fluence range of $\sim 10^{19}$ atoms/m^2. Considering the effect of fluence on hydrides emission on Al, we suggest that checking the production of hydrides from Be exposed to fusion relevant conditions during TPD experiments in line-of-sight configuration could be useful for the development of MRE models.

Declaration of interests

The authors declare that they have no known competing financial interests or personal relationships that could have appeared to influence the work reported in this paper.

Acknowledgments

The project leading to this publication has received funding from the Excellence Initiative of Aix-Marseille University - A*Midex, a French "Investissements d'Avenir" program. This work was also carried out within the framework of the EUROfusion Consortium and has received funding from the Euratom research and training program under grant agreement WP15-IPH-WPPFC1. The views and opinions expressed herein do not necessarily reflect those of the European Commission.

References

[1] R.W. Conn, et al., Fusion Eng. Des. 37 (1997) 481–513.
[2] G. Federici, et al., Comprehensive Nuclear Material, Elsevier, Konings, Amsterdam, 2012, p. 4.
[3] I. Bykov, et al., Nucl. Mater. Energy 12 (2017) 379–385.
[4] S. Ratynskaia, et al., Nucl. Fusion 58 (2018) 106023.
[5] L. Marot, et al., Fusion Eng. Des. 88 (2013) 1718–1721.
[6] A. Kreter, et al., Phys. Scr. T159 (2014) 014039.
[7] R.P. Doerner, et al., J. Nucl. Mater. 455 (2014) 1–4.
[8] C. Quiros, et al., Nucl. Mater. Energy 12 (2017) 1178–1183.
[9] K. Ouaras, et al., J. Phys. Conf. Ser. 159 (2015) 012029.
[10] G.S. Was, Fundamentals of Radiation Materials Science: Metals and Alloys, Springer, 2007.
[11] D. Connétable, et al., J. Alloys Compounds 748 (2018) 12.
[12] E.A. Hodille, Nucl. Fusion 57 (2017) 076019.
[13] R. Bisson, J. Nucl. Mater. 467 (2015) 432–438.
[14] C. Sang, et al., Nucl. Fusion 52 (2012) 043003.
[15] C. Sang, et al., J. Nucl. Mater. 463 (2015) 367–371.
[16] A. Winkler, J. Chem. Phys. 95 (1991) 7682.
[17] S. Kaur, et al., Phys. Rev. A 80 (2009) 042701.
[18] R. Behrish, Sputtering By Particle Bombardment II: Sputtering of Alloys and compounds, Electron and Neutron sputtering, Surface Topography 52 Springer, Germany, 1983.
[19] R.G. Saint Jacques, Nucl. Instr. Methods 209-210 (1983) 333–343.
[20] J.B. Condon, et al., J. Nucl. Mater. 207 (1993) 1–24.
[21] W.D. Calister, et al., Materials Science and Engineering: An Introduction, eight ed., John Wiley and Sons, United States, 2010.
[22] E. Serra, et al., J. Nucl. Mater 255 (1998) 105–115.
[23] D.E. Post, et al., Physics of Plasma-Wall Interactions in Controlled Fusion, first ed., Plenum Press, United States, 1986.
[24] S.J. Zinkle, Comprehensive Nuclear Materials, Chapter Radiation-Induced Effects on Microstructure, Elsevier, 2012, pp. 65–98.
[25] X.C. Ren, et al., Metall. Mater. Trans. A 39 (2008) 87–97.
[26] C. Wolverton, et al., Phys. Rev. B 69 (2004) 144109.
[27] V. Gavini, et al., Phys. Rev. B 76 (2007) 180101.
[28] H. Kawamura, et al., Mater. Trans. 42 (2001) 2175–2179.
[29] A. Winkler, et al., J. Chem. Phys. 95 (1991) 7682–7688.
[30] V. Lossev, et al., Surf. Sci. 284 (1993) 175–185.